Journal of Medicinal Chemistry

pubs.acs.org/jmc Article

Identification of the Clinical Development Candidate MRTX849, a Covalent KRAS^{G12C} Inhibitor for the Treatment of Cancer

Jay B. Fell,* John P. Fischer, Brian R. Baer, James F. Blake, Karyn Bouhana, David M. Briere, Karin D. Brown, Laurence E. Burgess, Aaron C. Burns, Michael R. Burkard, Harrah Chiang, Mark J. Chicarelli, Adam W. Cook, John J. Gaudino, Jill Hallin, Lauren Hanson, Dylan P. Hartley, Erik J. Hicken, Gary P. Hingorani, Ronald J. Hinklin, Macedonio J. Mejia, Peter Olson, Jennifer N. Otten, Susan P. Rhodes, Martha E. Rodriguez, Pavel Savechenkov, Darin J. Smith, Niranjan Sudhakar, Francis X. Sullivan, Tony P. Tang, Guy P. Vigers, Lance Wollenberg, James G. Christensen, and Matthew A. Marx*

Cite This: https://dx.doi.org/10.1021/acs.jmedchem.9b02052 Read Online

ACCESS | Metrics & More | Article Recommendations | Supporting Information

ABSTRACT: Capping off an era marred by drug development failures and punctuated by waning interest and presumed intractability toward direct targeting of KRAS, new technologies and strategies are aiding in the target's resurgence. As previously reported, the tetrahydropyridopyrimidines were identified as irreversible covalent inhibitors of KRAS^{G12C} that bind in the switch-II pocket of KRAS and make a covalent bond to cysteine 12. Using structure-based drug design in conjunction with a focused in vitro absorption, distribution, metabolism and excretion screening approach, analogues were synthesized to increase the potency and reduce metabolic liabilities of this series. The discovery of the clinical development candidate **MRTX849** as a potent, selective covalent inhibitor of KRAS^{G12C} is described.

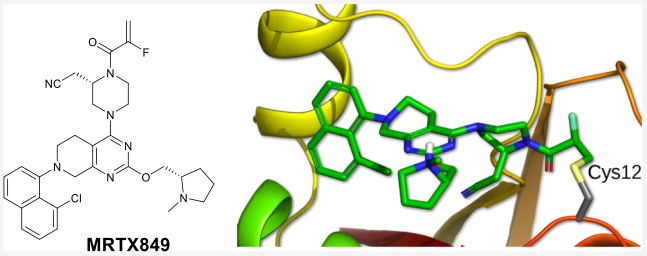

INTRODUCTION

KRAS is the single most frequently mutated oncogene and the first of more than 700 genes to be causally implicated in human cancer (COSMIC).[1] Mutations in *KRAS* are prevalent amongst the top three most deadly cancer types in the United States: pancreatic (95%), colorectal (45%), and lung (35%).[2] Its frequent mutation across a spectrum of aggressive cancers has stimulated an intensive drug discovery effort to develop therapeutic strategies that block KRAS function for cancer treatment. Despite nearly four decades of research, a clinically viable KRAS cancer therapy has remained elusive largely because of its high affinity for GTP and lack of a well-defined binding pocket.[3−6] However, recent findings have stimulated a new wave of activities to develop KRAS-targeted therapies.

Capping off an era marred by drug development failures and punctuated by waning interest and presumed intractability toward direct targeting of KRAS, new technologies and strategies are aiding in the target's resurgence.[7,8] Central to this renewal is a single mutation: KRAS^{G12C}, a well-validated driver mutation and the most frequent individual KRAS mutation in lung cancer.[4] Associated with poor prognosis and resistance to treatment, KRAS^{G12C} represents both an extraordinary unmet clinical need and opportunity. This mutation has a causal role in 14% of lung adenocarcinomas (~14,000 new US cases annually) and 5% of colorectal adenocarcinomas (~5000 new US cases annually) and is present in smaller fractions of other cancers. Collectively, KRAS^{G12C} mutations comprise a patient population with a worldwide annual incidence of greater than 100,000 individuals. A novel scientific basis for targeting KRAS^{G12C} was recently described in a breakthrough article by Shokat and Wells, in which they identified a previously unknown allosteric pocket near the nucleotide binding site.[9] Small molecules binding to this pocket can inhibit signaling through KRAS by locking the protein in its inactive GDP-bound state.[10−13] Although targeting this site with covalent, small-molecule inhibitors was a clear advancement, it was also evident that the molecules identified required significant optimization to achieve drug-like potency and pharmaceutical properties.

As previously reported, compound **1** (Figure 1) is an irreversible covalent inhibitor of KRAS^{G12C} that binds in the

Received: December 10, 2019

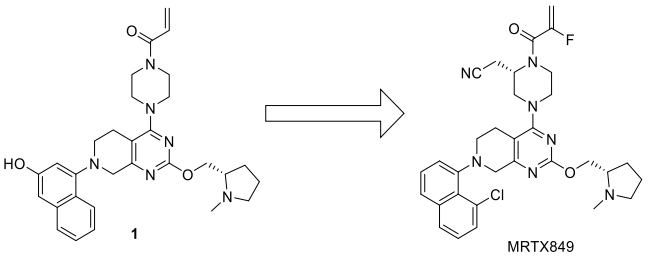

Figure 1. Structural comparison of compound **1** to clinical development candidate **MRTX849**.

switch-II pocket of KRAS and makes a covalent bond to cysteine 12.[14] Inhibitor **1** showed robust target engagement in a PK/PD experiment using MIA PaCa-2 tumor bearing mice when dosed IP. In a related tumor growth inhibition (TGI) experiment, compound **1** demonstrated rapid regressions with cures when dosed as low as 30 mg/kg IP once a day. While providing a valuable tool compound, inhibitor **1** demonstrated clearance (CL) of 46 mL/min/kg following a 3 mg/kg IV dose to CD-1 mice and oral bioavailability of 2.4% with a 100 mg/kg PO dose. The pharmacokinetic limitations of **1** necessitated several iterations of optimization to identify a tractable clinical candidate. Described in this paper are the insights that led to the discovery of the clinical candidate **MRTX849**.

RESULTS AND DISCUSSION

In order to advance the tetrahydropyridopyrimidine series of covalent $KRAS^{G12C}$ inhibitors, it was necessary to develop an understanding of the metabolic liabilities of **1** that contributed to high CL and low bioavailability in CD-1 mice. Compound **1** was incubated with mouse hepatocytes, and the metabolites were identified by liquid chromatography mass spectrometry (LCMS) with relative concentrations being estimated based on peak area in the corresponding A_{290nm} chromatogram (Table 1). The metabolism of naphthol is well-documented,[15] and it was not surprising that the hydroxyl moiety was the major metabolic liability for compound **1** with 76% of the identified metabolites being *O*-glucuronides (M1, M2, M6, and M7) or *O*-sulfate (M3). Glutathione (GSH) conjugation of the acrylamide also appeared to play an important role, 50% of the metabolites (M1, M2, M4, and M5) contained this modification.

Given the metabolite profile, it was predicted that removal of the hydroxyl moiety from compound **1** may decrease overall CL by reducing conjugative metabolism. As previously described,[14] the naphthol ring of this class of inhibitors binds in a well-defined hydrophobic pocket formed by Val9, Met72, Phe78, Tyr96, Ile100, and Val103. In addition, the naphthyl hydroxyl forms a hydrogen bond to the carboxylate of Asp69. Table 2 describes a series of substituted indazoles that were designed as naphthol replacements that fill the hydrophobic pocket while maintaining a hydrogen bonding interaction to Asp69. The activity of these compounds, reported as IC_{50} (nM), was determined in NCI-H358 cells by measuring inhibition of phospho-ERK after a 3 h incubation with the inhibitor. Because the intracellular drug disposition was unknown, the liabilities of conducting SAR studies using cellular data were recognized. The 5-methylindazole **2** displayed 1/10th of the cellular potency of compound **1**; this loss in potency was attributed to inadequate interactions with the protein. The 5-ethylindazole **3** and the 5-isopropylindazole **4** are equipotent to analogue **2** within variance of the assay. Through improved contact with the protein, both the 5-trifluoromethylindazole **5** and the 5,6-dimethylindazole **6** showed cellular IC_{50}'s approximately five fold more potent than compound **2**. As the most active of the naphthol replacements, the substituted indazoles **5** and **6** were profiled in a series of metabolic stability and permeability assays. While the human hepatocyte and microsome stability data were promising, with a hepatic extraction ratio (ER) of <55%, these analogues exhibited low permeability and were potent P-gp

Table 1. Metabolites of Compound 1 Identified in Incubations with Mouse Hepatocytes

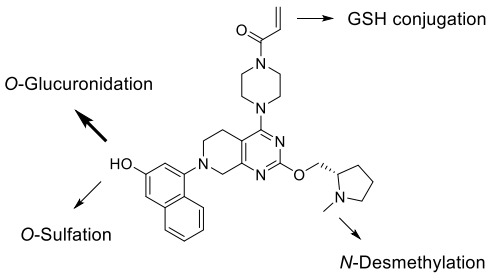

metabolite	biotransformation(s)	% peak area
M1	dealkylation; glucuronide; GSH	8
M2	glucuronide; GSH	18
M3	sulfate	9
M4	dealkylation; GSH	6
M5	GSH	14
M6	dealkylation; glucuronide	14
M7	glucuronide	27
Compound **1**		4

Table 2. Exploration of Substituted Indazoles as Hydroxy Naphthyl Replacements[a]

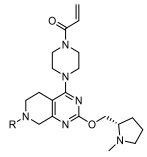

Compound	R	Cellular IC_{50} (nM)
1		142 ± 12
2		1500 ± 574
3		1080 ± 295
4		1180 ± 257
5	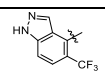	351 ± 89
6		254 ± 32

[a]NCI-H358 cellular pERK inhibition at 3 h.

https://dx.doi.org/10.1021/acs.jmedchem.9b02052
J. Med. Chem. XXXX, XXX, XXX−XXX

efflux substrates with permeability efflux (PE) ratios of 75 and 88, respectively. These results prompted the exploration of an alternate strategy for progressing the project.

Because the indazole analogues designed as naphthol replacements did not achieve acceptable cellular permeability, the hydroxyl moiety was targeted for removal in an effort to improve both permeability as well as metabolic stability. The deshydroxy analogue **7** was synthesized (Figure 2), and the PK

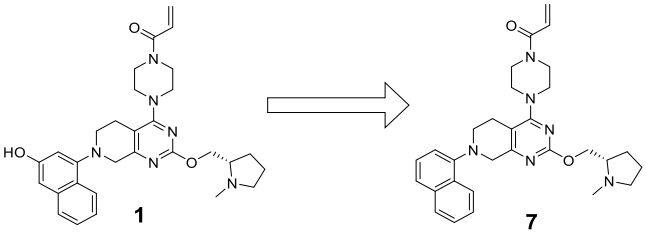

Figure 2. Compound **1** and the deshydroxy analogue **7**.

was evaluated in CD-1 mice. Following a 3 mg/kg IV dose of compound **7** to CD-1 mice (n = 3), CL was 25.6 mL/min/kg, the $t_{1/2}$ was 0.908 h, and the volume of distribution (V_{SS}) was 0.996 L/kg (Table 3). Oral administration of a 10 mg/kg dose

Table 3. PK of Compound 7 Dosed in CD-1 Mice

dose	parameter	value
3 mg/kg IV	CL (mL/min/kg)	25.6
	$t_{1/2}$ (h)	0.908
	V_{SS} (L/kg)	0.996
10 mg/kg PO	C_{max} (μg/mL)	0.131
	T_{max} (h)	0.500
	AUC_{inf} (h·μg/mL)	0.302
	F (%)	13.9

of **7** to mice (n = 3) resulted in a C_{max} of 0.131 μg/mL and AUC_{inf} of 0.302 h·μg/mL, with 13.9% bioavailability. The lower CL and higher bioavailability of **7** relative to **1**, albeit at a different dose, validated the decision to remove the hydroxyl metabolic liability. The weak cellular activity of compound **7** toward $KRAS^{G12C}$, IC_{50} = 4400 ± 73 nM compared to 142 ± 12 nM for compound **1**, prompted a search for additional interactions with the protein to move the series into a progressable activity range.

Figure 3 illustrates the X-ray crystal structure of compound **7** bound to $KRAS^{G12C}$. Notable in this structure is a bound water molecule complexed to Gly10 and Thr58 which is near the piperazine ring of compound **7**. This water molecule forms hydrogen bonds with the side chain hydroxyl of Thr58 (ca. 2.7 Å) and the carbonyl of Gly10 (3.0 Å), highlighted in Figure 3. The water is also ca. 3.0 Å from the backbone NH of Gly10. Analysis of the proximal hydrogen bonding network suggested that displacement of this water could lead to a large potency increase.[16] An appropriately substituted piperazine ring would have the correct trajectory to displace this bound water.

Table 4 describes a series of analogues that was synthesized to probe the space occupied by the Gly10-bound water. Substituents were placed at either R_1 or R_2 while keeping the other positions on the piperazine unsubstituted. Compounds **8**–**11** are a set of R_1- and R_2-substituted hydroxy methyl and hydroxy ethyl analogues that were designed to displace the bound water and replace the hydrogen bonding interactions in

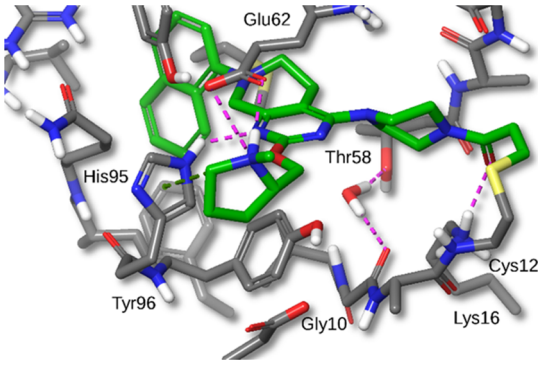

Figure 3. X-ray crystal structure of compound **7** bound to $KRAS^{G12C}$ with 2.27 Å resolution, hydrogens added for clarity (PDB code 6USX).

Table 4. Substituted Piperazines Designed To Displace $KRAS^{G12C}$ Gly10-Bound Water[a]

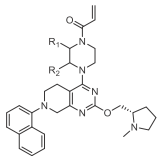

Compound	R_1	R_2	Cellular IC_{50} (nM)
7	H	H	4400 ± 73
8		H	4630 ± 175
9	H		4530 ± 1010
10		H	>5000 ± nd
11	H	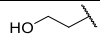	4840 ± 204
12		H	14 ± 3
12a		H	10 ± 2
12b		H	1020 ± 421
13	H		3320 ± 1080

[a]NCI-H358 cellular pERK inhibition at 3 h.

the pocket. These compounds were equal or less potent than the unsubstituted compound **7** in the NCI-H358 cell assay. Analogue **12**, substituted at the R_1 position with CH_2CN, showed a 300-fold increase in potency with a cellular IC_{50} = 14 nM. The diastereomers of **12** were synthesized, and the *S*-diastereomer **12a** was determined to be ∼100× more potent than the *R*-diastereomer **12b**. In addition to binding, another factor that could contribute to increased potency of a covalent inhibitor is electrophile reactivity. For example, compound **7** was incubated with GSH at 37 °C and the percent parent remaining at 1 and 4 h was measured. From these data, the half-life ($t_{1/2}$), a relative measure of electrophile reactivity, was extrapolated to be 17 h. Compound **12a**, on the other hand, had a GSH $t_{1/2}$ of 4 h, indicating that the electron withdrawing cyanomethyl substituent had the effect of increasing the

https://dx.doi.org/10.1021/acs.jmedchem.9b02052
J. Med. Chem. XXXX, XXX, XXX−XXX

reactivity of the acrylamide toward GSH. Interestingly, the opposite enantiomer **12b** also showed increased reactivity, GSH $t_{1/2}$ = 1 h. However, unlike **12a** which was 400× more potent than **7**, **12b** with a cell IC_{50} = 1020 nM was only 4 fold more potent than compound **7**. No increase in potency was observed with the cyanomethyl regioisomer **13**.

In addition to the potent cell activity, compound **12a** displayed favorable in vitro absorption, distribution, metabolism, and excretion (ADME) properties. This compound had 95% plasma protein binding such that the free fraction adjusted cell IC_{50} was calculated to be 200 nM. Compound **12a** had measured solubility of 800 μg/mL in FaSSIF at pH 6.5. CL in microsome preparations was modest, with an ER of 45% and high in hepatocytes, with an ER of 90%. This compound displayed medium permeability with efflux (P_{app} (A to B) = 2.2 × 10^{-6} cm/s, PE = 28) in the MDR LLCPK assay. Taken together, these data suggested that compound **12a** represented an interesting lead compound that warranted further investigation. Optimization of compound **12a** proceeded with substitution of the naphthalene moiety. Figure 4 shows a surface view of **12a** bound to $KRAS^{G12C}$ that

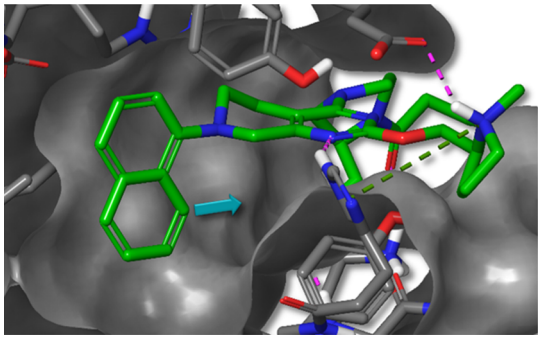

Figure 4. X-ray crystal structure of compound **12a** bound to $KRAS^{G12C}$ with 2.03 Å resolution, surface pose (PDB code 6USZ).

revealed a small pocket in the protein oriented from the 8-position of the naphthyl, highlighted with a blue arrow. A number of small hydrophobic groups were designed to fill this narrow hydrophobic cleft formed by residues Val9, Thr58, Met72, and Tyr96.

Following the synthetic route described in the Chemistry section, a series of analogues was synthesized to probe the vector from the naphthyl 8-position. The 8-substituted naphthyl compounds and their corresponding NCI-H358 cellular IC_{50} values are shown in Table 5. The methoxy and cyano analogues **14** and **15** were less potent compared to the proto analogue **12a**. 8-Ethyl naphthyl **16** and 8-trifluoromethyl naphthyl **17** displayed similar potency to the parent with single digit cellular IC_{50} values. Finally, both the chloro and methyl substituted compounds **18** and **19** were more potent with cellular IC_{50}'s of 1 nM.[17]

Pharmacokinetics of the chloro and the methyl substituted compounds **18** and **19** were evaluated in CD-1 mice (Table 6). Oral administration of a 30 mg/kg dose of compound **18** to mice (n = 3) resulted in a C_{max} of 2.46 μg/mL and AUC_{inf} of 2.27 h·μg/mL, with 16.9% bioavailability. Oral administration of a 30 mg/kg dose of compound **19** to mice (n = 3) resulted in a C_{max} of 1.66 μg/mL and AUC_{inf} of 4.91 h·μg/mL, with 31.1% bioavailability. Given the cellular potency and favorable oral exposure observed in mice, compounds **18** and **19** were progressed into efficacy studies.

Table 5. Exploration of 8-Naphthyl Position[a]

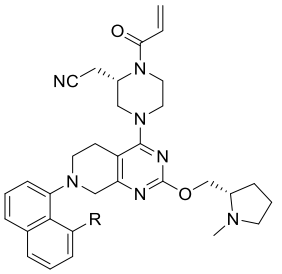

compound	R	cellular IC_{50} (nM)
14	methoxy	22 ± 7
15	cyano	64 ± 7
16	ethyl	6 ± 1
17	trifluoromethyl	4 ± 1
18	chloro	1 ± 0.1
19	methyl	1 ± 0.3

[a]NCI-H358 cellular pERK inhibition at 3 h.

Table 6. PK of Compounds 18 and 19 Dosed in CD-1 Mice

dose	parameter	18	19
3 mg/kg IV	CL (mL/min/kg)	37.3	31.6
	$t_{1/2}$ (h)	0.496	1.33
	V_{SS} (L/kg)	0.867	1.91
30 mg/kg PO	C_{max} (μg/mL)	2.46	1.66
	T_{max} (h)	0.250	0.500
	AUC_{inf} (h·μg/mL)	2.27	4.91
	F (%)	16.9	31.1

PK/PD studies were conducted to evaluate the pharmacodynamic response and to correlate drug exposure with target inhibition (Figure 5). Compounds **18** and **19** were

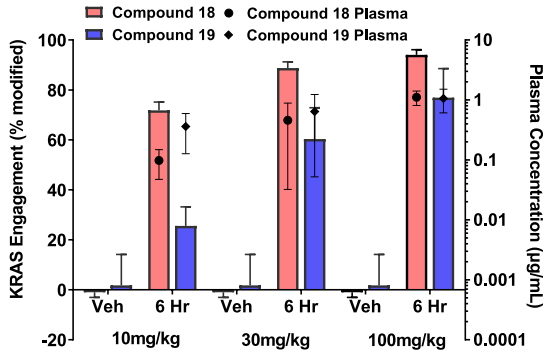

Figure 5. PK/PD of Compounds **18** and **19**.

administered via oral gavage over a range of dose levels to NCI-H358 xenograft-bearing mice. Tumors and plasma were collected 6 h after a single dose. Compound **18** showed 70% $KRAS^{G12C}$ modification at 10 mg/kg, 89% protein modification at 30 mg/kg, and >90% modification at 100 mg/kg as determined by LCMS analysis of the tumor lysate. In comparison, compound **19** exhibited 20, 60, and 80% modification at the same doses. Given the similarities between these two compounds, there was no clear explanation for the differences seen with in vivo target engagement. However, this study demonstrated a dose-dependent increase in covalent modification of $KRAS^{G12C}$ that was proportional to the plasma concentration of the drug for the individual compounds.[17]

https://dx.doi.org/10.1021/acs.jmedchem.9b02052
J. Med. Chem. XXXX, XXX, XXX−XXX

The antitumor activity of inhibitors **18** and **19** was evaluated in a MIA PaCa-2 xenograft TGI model (Figure 6). When

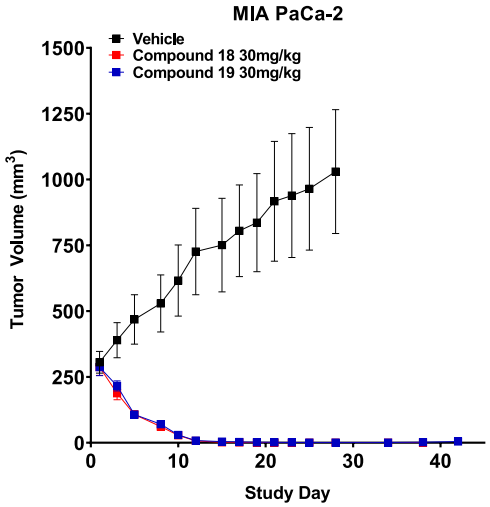

Figure 6. Antitumor Efficacy of Compounds **18** and **19**.

tumors reached ~350 mm^3, the compounds were administered daily via oral gavage until study day 16. Treatment with either compound **18** or **19** at 30 mg/kg resulted in significant and rapid tumor regression with evidence of complete responses that were durable after cessation of dosing. Although longer timepoints were not assessed in the current study, it should be noted that outgrowth was observed with compound **19**, dosed PO at 30 mg/kg, beginning 20 days after dosing ended in a previously presented study.[17]

Considering the robust efficacy observed in mouse PK/PD and TGI experiments, compounds **18** and **19** were progressed into second species pharmacokinetic studies. Subsequent to a 3 mg/kg IV dose in beagle dogs, both compounds exhibited high CL, high volume of distribution, and a $t_{1/2}$ of approximately 1 h. Following oral administration at a 10 mg/kg dose, these compounds exhibited 4% bioavailability with low plasma exposure, $AUC_{inf} \leq 0.04$ h·μg/mL (Table 7). Using the rodent

Table 7. PK of Compounds 18 and 19 in Beagle Dogs

dose	parameter	18	19
3 mg/kg IV	CL (mL/min/kg)	225	151
	$t_{1/2}$ (h)	0.826	0.966
	V_{SS} (L/kg)	7.91	6.16
10 mg/kg PO	C_{max} (μg/mL)	0.0163	0.0178
	t_{max} (h)	0.833	1.17
	AUC_{inf} (h·μg/mL)	0.0319	0.0395
	F (%)	4.12	3.67

and dog pharmacokinetic data, an allometric interspecies scaling approach described by Mahmood[18] was employed to predict human CL; values of 145 mL/min/kg (ER = 699%) and 121 mL/min/kg (ER = 588%) were calculated for **18** and **19**, respectively. The greater than liver blood flow[19] CL values that were measured in dogs and predicted in humans suggested that an extra-hepatic mechanism was contributing to the CL of compounds **18** and **19**.

Based on these observations and literature reports regarding the CL of targeted covalent inhibitors from Shibata and Chiba[20] and Leung,[21] it was likely that **18** and **19** were metabolized by either direct reaction with GSH or by GST-mediated GSH conjugation. To understand the mechanism of GSH conjugation onto the acrylamide, a diverse set of compounds from the tetrahydropyridopyrimidine series was subjected to reaction with GSH in phosphate buffer at 37 °C. A similar experiment using liver cytosol preparations plus GSH to capture GST/GSH-dependent conjugation also was run.[20] A lack of correlation between the two data sets, represented by the line of unity in Figure 7 (see Supporting Information for

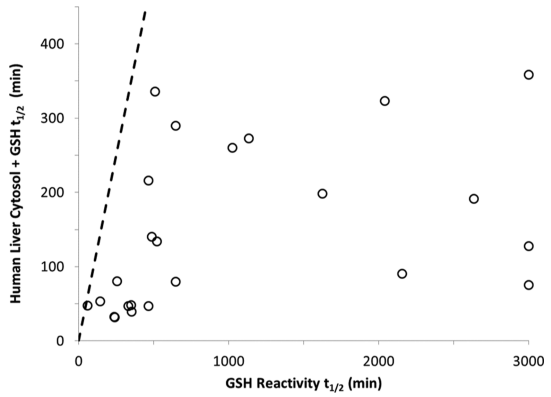

Figure 7. Comparison of inherent GSH reactivity to GST-mediated GSH metabolism in the human liver cytosol for a diverse set of tetrahydropyridopyrimidines.

data), and a lower $t_{1/2}$ toward GSH conjugation in liver cytosol compared to reactivity in buffer, suggested that the compounds were susceptible to GST-mediated GSH conjugation.

Further characterization of the GST isoforms responsible for GSH conjugation was performed. Confirmation of GSTA1-1-mediated GSH conjugation in the human liver cytosol was obtained. A linear correlation, R^2 = 0.76 between the liver cytosol preparation plus GSH and GSTA1-1 plus GSH in buffer, is shown in Figure 8 (see Supporting Information for data).

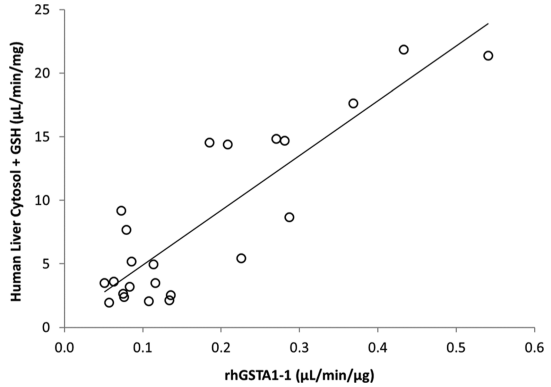

Figure 8. Correlation of CL values for the tetrahydropyridopyrimidine series between GSTA1-1-mediated metabolism and human liver cytosol.

In a similar fashion, GSTP1-1 was identified as the primary isoform responsible for mediated GSH conjugation in human whole blood (HWB). As shown in Figure 9 (see Supporting Information for data), the HWB stability assay provided a good correlation, R^2 = 0.66, to GST/GSH-dependent CL and was adopted as the primary metabolic stability assay.

https://dx.doi.org/10.1021/acs.jmedchem.9b02052
J. Med. Chem. XXXX, XXX, XXX−XXX

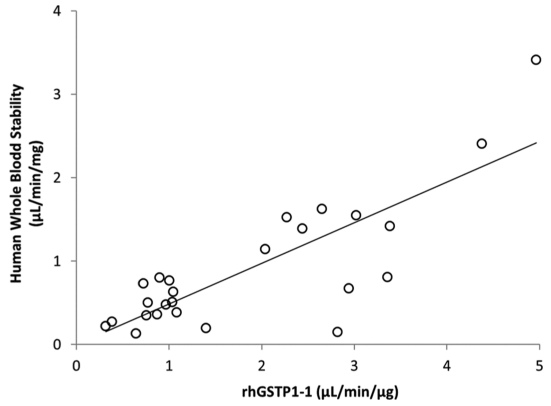

Figure 9. Correlation of CL values for the tetrahydropyridopyrimidine series between GSTP1-1-mediated metabolism and HWB stability.

As previously reported by Xia[22] and more recently by Zhao,[23] a substituted acrylamide electrophile can produce a potent covalent inhibitor with less reactivity toward GSH compared to the unsubstituted counterpart. Considering the greater target engagement observed with compound **18** compared to compound **19** in the previously described PK/PD experiment, a set of analogues designed around inhibitor **18** was synthesized with substituted acrylamides. Shown in Table 8, the reference unsubstituted compound **18** was a 1 nM

Table 8. Substituted Electrophiles to Attenuate Reactivity[a]

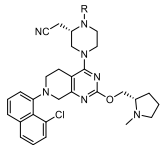

Compound	R =	Cellular IC_{50} (nM)	WB Stability $T_{1/2}$ (hours) mouse/dog/human
18		1 ± 0.1	5/2/14
20		14 ± 3	>50/>50/>50
21		>5000	>50/>50/40
22		3 ± 1	11/9/>50
23		9 ± 3	11/22/>50

[a]NCI-H358 cellular pERK inhibition at 3 h.

cellular inhibitor with measured WB stability of 5/2/14 h across species (mouse/dog/human). Compound **20** contained a 2-fluoro acrylamide substituent; this substitution resulted in a decrease in cell potency but with a concomitant improvement in WB stability to >50 h across species. The 2-methoxy analogue **21** was inactive in the cell assay. The 3-substituted analogues, **22** and **23**, had cellular IC_{50} < 10 nM. However, although they showed improved stability in the WB assay relative to compound **18**, these compounds exhibited shorter half-lives than the 2-fluoro inhibitor **20**.

As a result of its much reduced GST-mediated GSH conjugation, compound **20** (**MRTX849**) was further characterized in vitro and advanced into in vivo efficacy studies. Calculated and measured properties of **MRTX849** are shown in Table 9. Highlighting in vitro ADME, **MRTX849** showed

Table 9. Properties of MRTX849

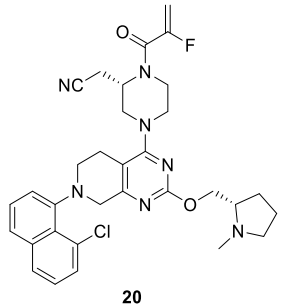

20
MRTX849

MW/Clog *P*/PSA (Å^2)	604/5.8/87
NCI-H358 cellular IC_{50} @ 3 h (nM)	14
MIA PaCa-2 cellular IC_{50} @ 24 h (nM)	5
permeability AB 10^{-6} cm/s, PE	4.7, 56
hepatocyte ER % (m, d, h)	61, 36, 50
microsome ER % (m, d, h)	57, 39, 56
whole blood stability $t_{1/2}$ (h)	>50
plasma protein binding % (m, h)	99.0, 98.3
FaSSIF solubility pH 6.5 μg/mL	568

moderate permeability with an AB value of 4.7 × 10^{-6} cm/s and displayed efflux in the MDR-LLCPK transfected line. Moderate stability in hepatocytes and microsomes was observed across the species tested, and the whole blood $t_{1/2}$ was greater than 50 h in all species.

Co-crystal structures generated throughout lead optimization of the tetrahydropyridopyrimidine series provided insight toward new analogue design. Key findings are illustrated by the high-resolution X-ray crystal structure of **MRTX849** bound to $KRAS^{G12C}$ shown in Figure 10. The interatomic distance of 1.65 Å between the Cys12 sulfur and the acrylamide β-carbon is consistent with a covalent bond. Key polar interactions include hydrogen bonds between the amine nitrogen of Lys16 and the acrylamide carbonyl (3.0 Å), the NE2 nitrogen of

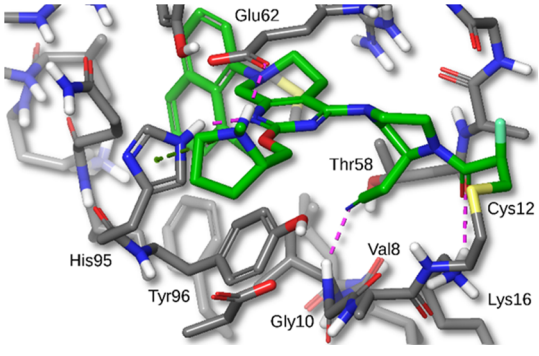

Figure 10. X-ray crystal structure of **MRTX849** bound to $KRAS^{G12C}$ with 1.94 Å resolution, hydrogens added for clarity (PDB code 6UT0).

https://dx.doi.org/10.1021/acs.jmedchem.9b02052
J. Med. Chem. XXXX, XXX, XXX−XXX

His95, and N-1 of the pyrimidine ring (2.9 Å). The C-2 pyrrolidine forms a salt-bridge with the carboxylate of Glu62, N−O distance of 2.8 Å. The cyanomethyl substituent displaces the Gly10 bound water and forms a hydrogen bond to the backbone NH of Gly10 (N−N distance 3.3 Å). Interestingly, displacement of the water via the cyanomethyl substituent also causes the chi1 angle of Thr58 to rotate from ca. 65° in compound **7** to −53° in **MRTX849**, and the side chain hydroxyl forms an H-bond with the backbone carbonyl of Val8, most likely due to loss of the H-bond with water. The methyl of Thr58 provides for more hydrophobic contacts with this class of inhibitors. The 8-chloronaphthyl fills the lipophilic pocket as previously discussed. Other key hydrophobic interactions are identical to those previously noted.[15]

The kinetics of $KRAS^{G12C}$ modification by **MRTX849** were evaluated to understand how the reversible affinity (K_I), the rate of inactivation (k_{inact}), and the overall potency (k_{inact}/K_I) compare with other $KRAS^{G12C}$ covalent inhibitors. Following treatment of $KRAS^{G12C}$ with **MRTX849**, the rates of target engagement (k_{obs}) were determined by LCMS measurement of the pepsin-derived Cys12-containing peptide fragments (Figure 11). The k_{inact} and K_I values determined from three

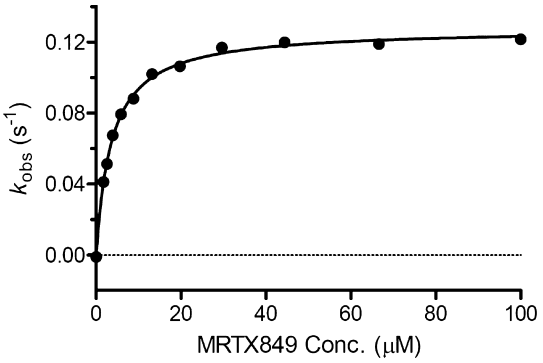

Figure 11. k_{inact}/K_I determination for **MRTX849**. Data represent the mean k_{obs} measured from three experiments.

separate experiments were 0.13 ± 0.01 s^{-1} and 3.7 ± 0.5 μM, respectively. The k_{inact}/K_I value for **MRTX849** was calculated to be 35 ± 0.3 mM^{-1} s^{-1} compared to the $KRAS^{G12C}$ inhibitors ARS-1620 (1.1 mM^{-1} s^{-1})[24] and AMG 510 (9.9 mM^{-1} s^{-1})[25] found in the literature.

The selectivity of **MRTX849** toward Cys12 of $KRAS^{G12C}$ was evaluated in NCI-H358 cells. Guided by the methodology described by Patricelli,[12] a thiol-reactive probe was used to profile the cysteine residues in the proteome with and without 3 h treatment of 1 μM **MRTX849**. The results of this experiment, represented in Figure 12, show the treated versus control peptide ratio plotted for the 5702 identified peptides. The peptide-containing Cys12 of $KRAS^{G12C}$ had a peptide ratio of 0.03 following treatment with **MRTX849**, indicating nearly complete engagement of the intended target. Lysine-tRNA ligase (gene = *KARS*) was the only off target protein that was identified in this study. These data demonstrated that **MRTX849** showed highly specific modification of $KRAS^{G12C}$ in the NCI-H358 proteome at a concentration of 1 μM.

In a complementary chemical proteomics experiment, the specificity of **MRTX849** was characterized utilizing the alkyne-containing click probe analogue **24** (cellular IC_{50} = 140 ± 34 nM) to bait the protein targets (Figure 13). This experiment had the potential to identify lower abundance protein targets in

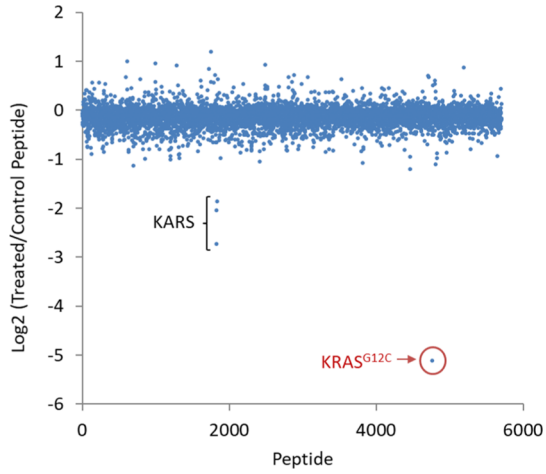

Figure 12. **MRTX849**-targeted proteins identified by MS-based proteomic cysteine profiling.

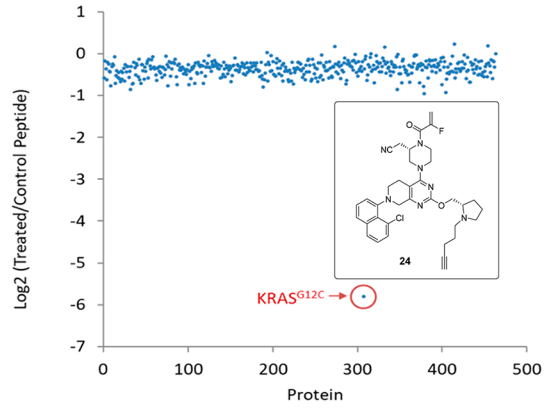

Figure 13. Click chemistry target identification in NCI-H358 cells using compound **24**.

comparison to the global cysteine reactivity experiment.[26] Of the 463 proteins that were identified and quantitated, only $KRAS^{G12C}$ significantly decreased in response to 1 μM **MRTX849** treatment, again confirming a high degree of selectivity for $KRAS^{G12C}$ (Figure 13).

The progression of the covalent $KRAS^{G12C}$ inhibitor **MRTX849** into pharmacokinetic studies in mouse, rat, and dog is detailed in Table 10. Key intravenous and oral pharmacokinetic parameters were determined using a non-compartmental approach and were calculated for these species. Results from this analysis indicated that improved WB stability translated into increased in vivo stability and exposure with the 2-fluoro acrylamide **MRTX849** when compared to analogue **18**.

Table 10. Single Dose IV and PO Mean Pharmacokinetic Parameters of MRTX849 Across Animal Species

dose	parameter	mouse	rat	dog
3 mg/kg IV	CL (mL/min/kg)	19.9	44.2	29.6
	$t_{1/2}$ (h)	1.51	2.57	7.56
	V_{SS} (L/kg)	2.02	20.7	17.4
30 mg/kg PO	C_{max} (μg/mL)	2.41	0.209	0.252
	T_{max} (h)	1.00	2.67	4.00
	AUC_{inf} (h·μg/mL)	15.9	2.67	4.47
	F (%)	62.9	29.7	25.9

https://dx.doi.org/10.1021/acs.jmedchem.9b02052
J. Med. Chem. XXXX, XXX, XXX−XXX

The moderate-to-high oral bioavailability observed across species, F = 25.9−62.9%, suggested the potential for similar oral bioavailability in human studies. Predicted human CL for **MRTX849** using an allometric scaling approach[18] indicated a CL value of 19 mL/min/kg, 7.6-fold lower predicted human CL value relative to compound **18**. The metabolism of **MRTX849** was characterized in hepatocytes across species (Supporting Information). In comparison to compound **1**, **MRTX849** formed fewer GSH adducts and no glucuronides. Based on MSMS fragmentation data, all oxidations occurred on the methylpyrrolidine group, and two metabolites were confirmed with synthetic standards; M10 was the *N*-dimethyl pyrrolidine metabolite and M11 was the methylpyrrolidin-2-one metabolite. Metabolite profiles were similar between preclinical species and humans. However, GSH conjugation was relatively minor in human hepatocytes compared to other species, suggesting that human CL may be overestimated by simple allometry.

PK/PD studies were conducted with **MRTX849** to evaluate the pharmacodynamic response and correlate drug exposure with target engagement. **MRTX849** was administered via oral gavage over a range of dose levels to NCI-H358 xenograft-bearing mice. Tumors and plasma were collected 6 h after a single dose. Shown in Figure 14, the fraction of covalently

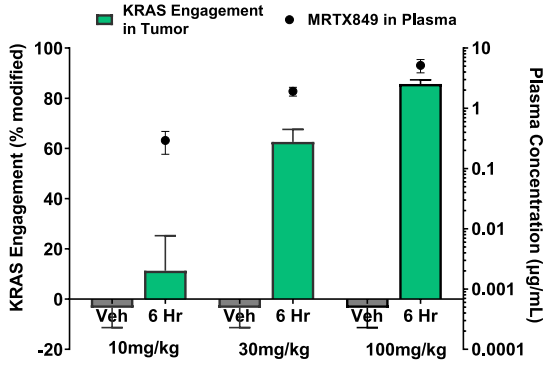

Figure 14. PK/PD of **MRTX849**.

modified $KRAS^{G12C}$ protein was proportional to the plasma concentration of **MRTX849**. This study demonstrated a dose-dependent increase in covalent modification of $KRAS^{G12C}$ by **MRTX849** with maximal modification achieved at a 100 mg/kg dose.[27]

The anti-tumor activity of **MRTX849** as evaluated in a MIA PaCa-2 xenograft model is shown in Figure 15. When tumors reached ∼350 mm^3, **MRTX849** was dosed daily via oral gavage until study day 16. Tumor regressions were seen in the 10 mg/kg dose group with rapid rebound observed following the end of dosing. Treatment at 30 and 100 mg/kg resulted in significant and rapid tumor regression, with evidence of complete responses that were durable after cessation of dosing. All mice in the 100 mg/kg cohort remained tumor-free for the duration of the study, and 2 of 7 mice in the 30 mg/kg cohort remained tumor-free through study day 70. In addition, drug treatment was well-tolerated with no loss of body weight at any dose level. These studies indicated that **MRTX849** demonstrated dose-dependent anti-tumor efficacy over a well-tolerated dose range and that the maximally efficacious dose of **MRTX849** in tumor bearing mice was between 30 and 100 mg/kg/day.[27]

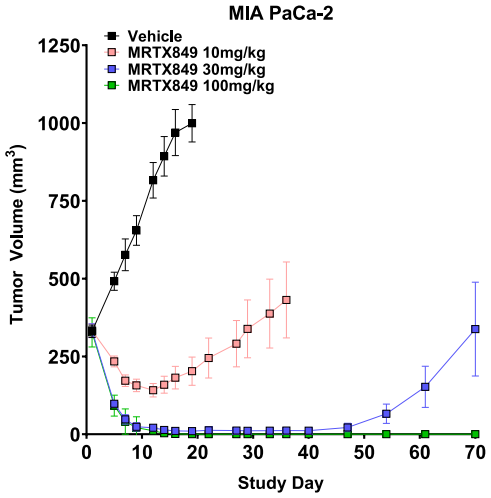

Figure 15. Antitumor Efficacy of **MRTX849**.

Chemistry. The synthesis of compound **1** (Scheme 1) commenced with the condensation of ethyl 1-benzyl-3-oxopiperidine-4-carboxylate and urea to form the bicyclic di-one core followed by chlorination with $POCl_3$ to provide 7-benzyl-2,4-dichloro-5,6,7,8-tetrahydropyrido[3,4-*d*]pyrimidine **25**. A two-step sequence to install the piperazine substituent at C4 and then the ether at C2 began with S_NAr reaction between the dichloro core and *N*-BOC piperazine in dimethyl sulfoxide (DMSO) at 50 °C. This S_NAr product was subjected to a coupling reaction under Buchwald conditions[28] with (*S*)-prolinol using RuPhos/Pd_2dba_3 as the catalyst to afford *tert*-butyl (*S*)-4-(7-benzyl-2-((1-methylpyrrolidin-2-yl)methoxy)-5,6,7,8-tetrahydropyrido[3,4-*d*]pyrimidin-4-yl)piperazine-1-carboxylate **26**. *N*-Benzyl group deprotection under hydrogenation conditions followed by introduction of the naphthyl moiety by Buchwald amination with 3-(benzyloxy)-1-bromonaphthalene gave intermediate **27**. Global deprotection and acylation with acryloyl anhydride resulted in the desired product **1**.

The synthesis of compounds **2**−**6** followed the same synthetic route as was used for compound **1**. Advanced intermediate **26** was deprotected by hydrogenation, then subjected to Buchwald amination reactions with the appropriately functionalized THP protected indazole using RuPhos/Pd_2dba_3 as the catalyst to give the nitrogen-arylated product (Scheme 2). Deprotection of both indazole and piperazine nitrogens was achieved by treatment with a solution of TFA in DCM. Installation of the acrylamide warhead using acryloyl anhydride gave the fully elaborated analogues. In addition, a similar synthetic sequence, substituting 1-bromonaphthalene for 3-(benzyloxy)-1-bromonaphthalene, was used to generate compound **7** (Scheme 3).

An alternate synthetic approach was devised for the synthesis of the substituted piperazines **8**−**13** that allowed for late stage diversification at C4. Following the route shown in Scheme 4, the synthesis of compound **12a** began with selective derivatization at C4 by treatment of intermediate **25** with sodium methoxide in methanol. The C2 prolinol side chain was installed using a Buchwald coupling that was followed by benzyl hydrogenolysis to give compound **28** in good yield. Installation of the naphthyl ring system was accomplished by Buchwald amination with 1-bromonaphthalene to give (*S*)-4-methoxy-2-((1-methylpyrrolidin-2-yl)-

https://dx.doi.org/10.1021/acs.jmedchem.9b02052
J. Med. Chem. XXXX, XXX, XXX−XXX

Scheme 1. Synthesis of Compound 1[a]

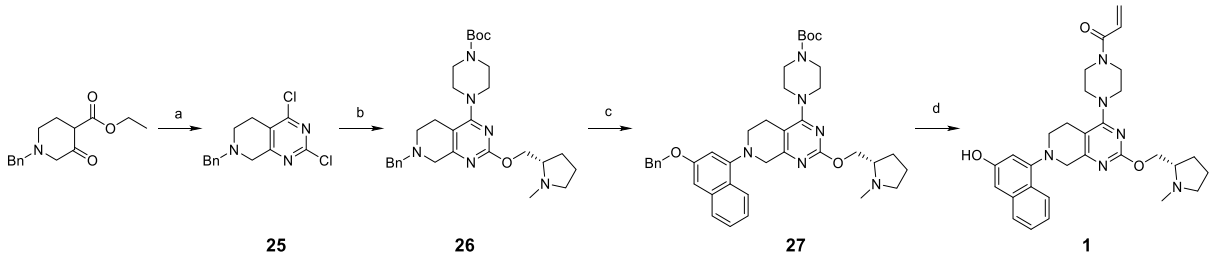

[a]Reagents and conditions. (a) (i) urea, NaOEt/EtOH, 80 °C, 21 h, 62%; (ii) $POCl_3$, 110 °C, 12 h, 60%; (b) (i) Boc-piperazine, DIEA, DMSO, 55 °C, 10 h, 80%; (ii) (*S*)-(1-methylpyrrolidin-2-yl)methanol, BINAP, $Pd(OAc)_2$, Cs_2CO_3, tol. 110 °C, 6 h, 90%; (c) (i) $Pd(OH)_2$, H_2, MeOH, 40 °C, 24 h, 94%; (ii) 3-(benzyloxy)-1-bromonaphthalene, RuPhos, $Pd_2(dba)_3$, Cs_2CO_3, tol., 110 °C, 70%; (d) (i) Pd/C, H_2, MeOH; (ii) HCl, MeCN, 0.5 h; (iii) acryloyl anhydride, DCM, DIEA, −50 °C, 12%.

Scheme 2. Representative Synthetic Route to the Indazole Analogues 2−6[a]

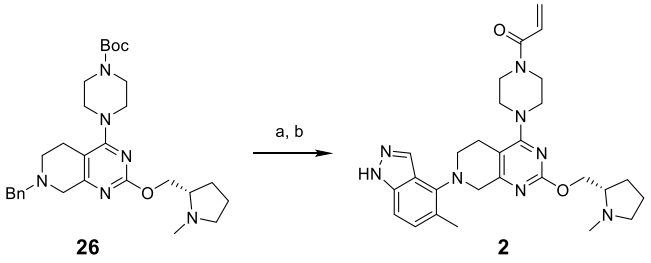

[a]Reagents and conditions. (a) (i) $Pd(OH)_2$, H_2, MeOH, 40 °C, 24 h, 94%; (ii) bromo-5-methyl-1-(tetrahydro-2*H*-pyran-2-yl)-1*H*-indazole, RuPhos, $Pd_2(dba)_3$, Cs_2CO_3, tol., 110 °C, 12 h, 70%; (b) (i) TFA, DCM, 1 h; (ii) acryloyl anhydride, DCM, DIEA, −40 °C, 49%.

Scheme 3. Synthesis of Compound 7[a]

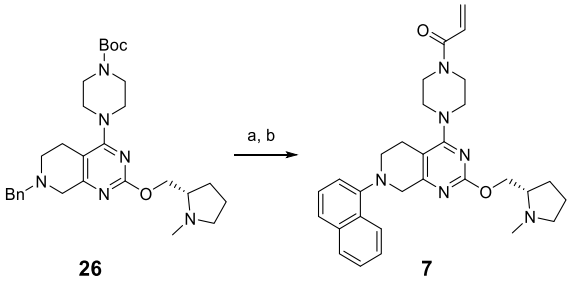

[a]Reagents and conditions. (a) (i) $Pd(OH)_2$, H_2, MeOH, 40 °C, 24 h, 94%; (ii) 1-bromonaphthalene, $Pd_2(dba)_3$, RuPhos, Cs_2CO_3, tol., 90 °C, 8 h, 87%; (b) (i) HCl, MeCN, HCl/dioxane, 30 min, 0 °C; (ii) acryloyl anhydride, DCM, DIEA, −40 °C, 10 min, 14% over 2 steps.

methoxy)-7-(naphthalen-1-yl)-5,6,7,8-tetrahydropyrido[3,4-*d*]-pyrimidine. Deprotection of this intermediate using a mixture of ethane thiol and sodium hydride in DMF followed by triflate formation with triflic anhydride and triethyl amine at reduced temperature gave compound **29**. The substituted piperazine was installed by S_NAr reaction of **29** with 2-piperazin-2-ylacetonitrile giving rise to the penultimate intermediate. Warhead attachment onto the piperazine nitrogen was accomplished by reaction with acryloyl anhydride, and subsequent separation of the diastereomers by chiral SCF chromatography gave **12a** and **12b**. Although the general approach to the synthesis of compounds **8−13** was the same as compound **12a**, modifications to the S_NAr reaction to install the substituted piperazine and final protecting group manipulations were necessary (see Supporting Information for details).

Shown in Scheme 5 is a convergent sequence to derivatize the 8-position of the naphthyl ring system while maintaining a Boc-protecting group at the piperazine nitrogen prior to warhead installation. The protecting group exchange at the nitrogen of ethyl 1-benzyl-3-oxo-piperidine-4-carboxylate from benzyl to Cbz was accomplished using a deprotection/reprotection sequence. Bicyclic ring formation was performed by treatment of 1-benzyl 4-ethyl 3-oxopiperidine-1,4-dicarboxylate with methyl carbamimidothioate. Triflate formation at C4 was accomplished by reaction of the C4 OH with triflic anhydride at reduced temperature to give **30**. S_NAr reaction upon treatment of **30** with (*S*)-2-(piperazin-2-yl)acetonitrile followed by protection of the free piperazine NH using Boc anhydride under standard conditions gave intermediate **31**. *m*-CPBA oxidation of the thiomethyl group at C2, S_NAr with (*S*)-prolinol and sodium *t*-butoxide and removal of the Cbz group under hydrogenation conditions provided **32**. Naphthyl installation, Boc-deprotection, and acrylamide formation were achieved as previously described to afford compound **19**.

An alternative strategy, detailed in Scheme 6, was devised for the formation of the 8-chloro substituted compound **18**. In a synthesis similar to that described for compound **12a**; **27** was treated under Buchwald amination conditions with 1-bromo-8-chloronaphthalene to give the N-arylated product. Demethylation at the C4 position and subsequent triflate formation provided **32**. Introduction of the chiral (*S*)-2-(piperazin-2-yl)acetonitrile by S_NAr reaction and warhead installation gave **18**.

Scheme 7 depicts the synthesis of compound **20** from the advanced intermediate **34** using T3P[29] as the coupling reagent to facilitate formation of the amide linkage with the acid coupling partner. Compounds **21−22** were synthesized in a similar fashion.

Synthesis of the click probe **24** was initiated by treatment of ethyl 1-benzyl-3-oxopiperidine-4-carboxylate with methyl carbamimidothioate and sodium ethoxide in ethanol to form the bicyclic ring system. Activation of the 4-position with $POCl_3$, S_NAr with (*S*)-2-(piperazin-2-yl)acetonitrile and subsequent protection of the free amine with Boc anhydride gave intermediate **35**. Benzyl deprotection of compound **35** followed by Buchwald amination using XantPhos and $Pd_2(dba)_3$ provided compound **36**. Oxidation of the thiomethyl substituent, displacement of the sulfoxide with (*S*)-(1-(pent-4-yn-1-yl)pyrrolidin-2-yl)methanol, and a two-

https://dx.doi.org/10.1021/acs.jmedchem.9b02052
J. Med. Chem. XXXX, XXX, XXX−XXX

Scheme 4. Representative Synthesis of Substituted Piperazines 8−13[a]

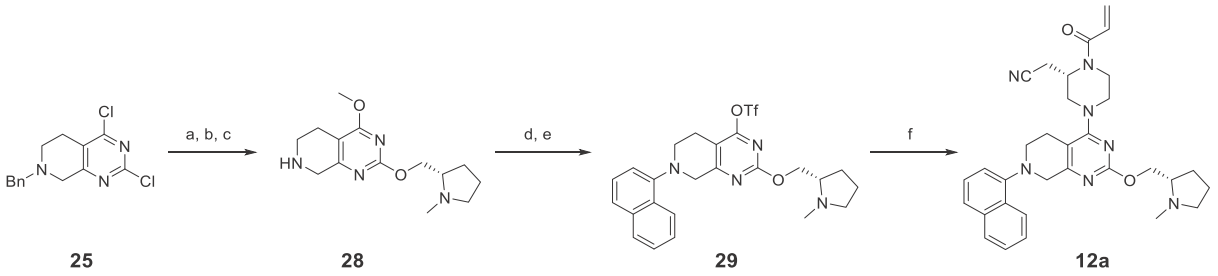

[a]Reagents and conditions. (a) NaOMe/MeOH 0 → 25 °C, 30 min, 92%; (b) (*S*)-(1-methylpyrrolidin-2-yl)methanol, BINAP, $Pd(OAc)_2$, Cs_2CO_3, tol., 110 °C, 8 h, 83%; (c) $Pd(OH)_2/C$, H_2, MeOH, 40 °C 48 h, 90%; (d) 1-bromonaphthalene, $Pd_2(dba)_3$, RuPhos, Cs_2CO_3, tol., 90 °C, 12 h, 64%; (e) (i) EtSH, NaH, DMF, 1 h (ii) DCM, TEA, 4 Å MS, Tf_2O, −40 °C, 22%; (f) (i) (*S*)-2-(piperazin-2-yl)acetonitrile, DIEA, DMA; (ii) acryloyl anhydride, DCM, DIEA, 0 °C, 1 h; (iii) SCF separation.

Scheme 5. Synthesis of 8-Substituted Naphthyl 14−17 and 19[a]

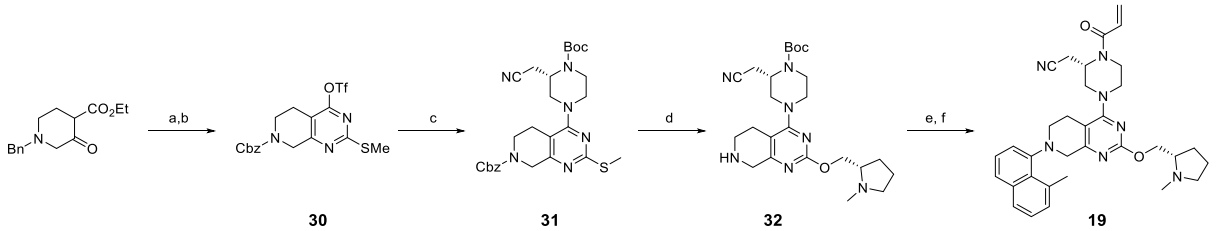

[a]Reagents and conditions. (a) (i) H_2, $Pd(OH)_2$, MeOH, 40 °C; (ii) CbzCl, DCM DIEA, 0 °C 36%; (b) (i) methyl carbamimidothioate, NaOMe/MeOH, 30 °C, 12 h, 85%; (ii) DCM, TEA, Tf_2O, −40 °C, 67%; (c) (i) (*S*)-2-(piperazin-2-yl)acetonitrile, DIEA, DMA, 80 °C, 83%; (d) (i) *m*-CPBA, DCM, 30 min, 89%; (ii) (*S*)-(1-methylpyrrolidin-2-yl)methanol, NaOtBu, tol., 0 °C, 6 h, 61%; (iii) Pd/C, H_2, MeOH, 40 °C, 24 h, 71%; (e) (i) 8-methyl, 1-bromonaphthalene, XantPhos, $Pd_2(dba)_3$, Cs_2CO_3, tol., 100 °C, 5 h, 59%; (ii) HCl diox/ACN, 30 min; (f) acryloyl anhydride, DCM, DIEA, −40 °C, 24%.

Scheme 6. Synthesis of Compound 18[a]

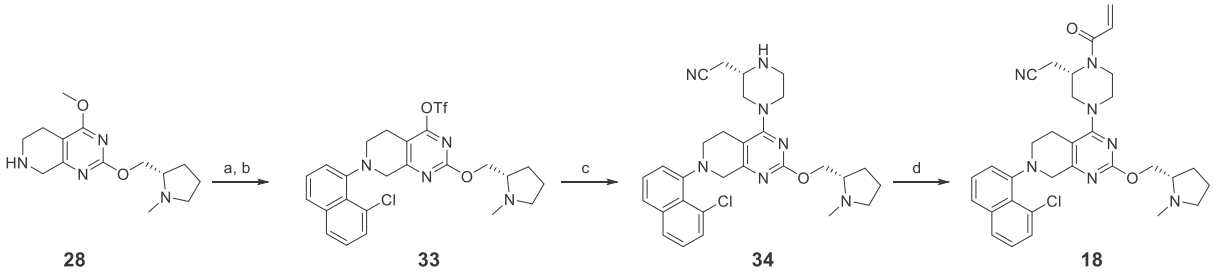

[a]Reagents and conditions. (a) $Pd_2(dba)_3$, RuPhos, Cs_2CO_3, tol. 90 °C, 12 h, 53%; (b) (i) EtSH, NaH, DMF, 60 °C, 1.5 h, 94%; (ii) Tf_2O, TEA, 4 Å MS, DCM, −40 °C, 30 min, 22%; (c) (*S*)-2-(piperazin-2-yl)acetonitrile, DIEA, DMA, rt, 15 min, 44%; (d) acryloyl chloride, DCM −40 °C, 10 min, 36%.

Scheme 7. Synthesis of the Clinical Candidate 20 (MRTX849)[a]

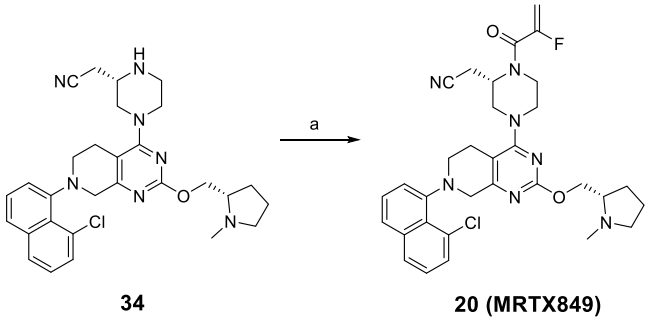

[a]Reagents and conditions. (a) 2-Fluoroprop-2-enoic acid, T3P, TEA, 0 °C, 30 min, 29%.

step deprotection/acylation sequence yielded click probe **24** (Scheme 8).

CONCLUSIONS

Insights leading to the discovery of the development candidate **MRTX849** began with the finding that removal of the hydroxyl moiety from **1** resulted in a five-fold improvement in oral bioavailability. Optimization of the deshydroxy analogue **7** to increase potency was predicated on the important observation that a bound water molecule was complexed to Gly10 and Thr58 in the crystal structure of **7** complexed to $KRAS^{G12C}$. Analysis of the proximal hydrogen bonding network suggested that displacement of this water could lead to a dramatic increase in potency. A series of analogues designed and synthesized to displace the Gly10 water culminated in the cyanomethyl-substituted piperazine **12a**. The NCI-H358

https://dx.doi.org/10.1021/acs.jmedchem.9b02052
J. Med. Chem. XXXX, XXX, XXX−XXX

Scheme 8. Synthesis of Click Chemistry Probe 24[a]

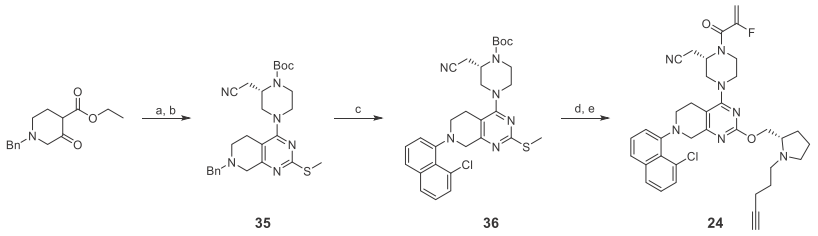

[a]Reagents and Conditions. (a) (i) ACE-Cl, DCE, 1 h, 0 °C; MeOH, 70 °C, 1 h, 82%; (ii) 8-chloro, 1-bromonaphthalene, 4 Å MS, XantPhos, $Pd_2(dba)_3$, Cs_2CO_3, tol., 110 °C, 12 h, 66%; (b) (i) *m*-CPBA, DCM, 30 min; (ii) (*S*)-(1-(pent-4-yn-1-yl)pyrrolidin-2-yl)methanol, NaOtBu, tol., 4 Å MS, 0 °C, 30 min, 64%; (c) (i) TFA, DCM; (ii) 2-fluoroprop-2-enoic acid, EtOAc, T3P, TEA, 0 °C, 30 min, 24%.

cellular IC_{50} of 10 nM represented a 400× potency boost for this inhibitor compared to compound **7**. Based on the GSH reactivity data of these compounds and **12b**, the large increase in potency was attributed to the displacement of the bound water molecule and the formation of new hydrogen bonding interactions with $KRAS^{G12C}$ rather than an overt increase in electrophile reactivity. Further optimization of **12a** yielded the 8-chloro analogue **18** with a cellular IC_{50} value of 1 nM. Following oral administration at 10 mg/kg to beagle dogs, compound **18** showed 4% bioavailability and insufficient projected human exposure to inhibit $KRAS^{G12C}$. A third key finding for the program was realized from a set of in vitro GSH conjugation experiments which were run in the presence of GST isoforms that confirmed that the tetrahydropyridopyrimidine compounds were undergoing GST-mediated GSH-conjugation. In order to minimize GSH metabolism, the development candidate **MRTX849** employed a 2-fluoroacrylamide warhead imparting whole blood stability of >50 h $t_{1/2}$ across species while maintaining tractable cellular potency (IC_{50} = 5−14 nM). Metabolism studies of **MRTX849** in hepatocytes showed that GSH conjugation of the 2-fluoroacrylamide was reduced compared to previous analogues containing the unsubstituted acrylamide. Favorable in vitro ADME and physical properties of **MRTX849** translated into moderate to high bioavailability of 26−63% across species tested. In a PK/PD experiment dosed at 10, 30, and 100 mg/kg to NCI-H358 tumor bearing mice, **MRTX849** demonstrated dose-dependent protein modification with nearly maximal effect at the highest doses. This compound was evaluated in a MIA PaCa-2 xenograft model orally administered at 10, 30, and 100 mg/kg QD for 16 days with continued post-treatment monitoring for a total of 70 days. **MRTX849** treatment in this study resulted in significant and rapid tumor regression with evidence of durable complete responses. The animals that were dosed at 100 mg/kg remained tumor-free for the duration of the 70-day monitoring period. Additionally, exquisite selectivity for $KRAS^{G12C}$ was observed in complimentary proteomics experiments: a biotin-streptavidin pull down study and a click probe experiment using a compound closely related to **MRTX849**. In conclusion, **MRTX849** is a potent, selective, orally bioavailable, irreversible covalent inhibitor of $KRAS^{G12C}$ with robust target engagement consistent with durable complete responses in tumor-bearing mice.

EXPERIMENTAL SECTION

General Chemistry Methods. All final compounds were purified to ≥95% purity by either high-performance liquid chromatography (HPLC) or supercritical fluid chromatography (SFC) and were characterized by proton NMR, carbon NMR, and high-resolution mass spectrometry as described below. All chemicals were purchased from commercial suppliers and used as received unless otherwise indicated. Proton nuclear magnetic resonance (^{1}H NMR) spectra were recorded on Bruker AVANCE 400 MHz spectrometers. Chemical shifts are expressed in δ ppm and are calibrated to the residual solvent peak: proton ($CDCl_3$, 7.27 ppm). Coupling constants (J), when given, are reported in hertz. Multiplicities are reported using the following abbreviations: s = singlet, d = doublet, dd = doublet of doublets, t = triplet, q = quartet, m = multiplet (range of multiplet is given), br = broad signal, and dt = doublet of triplets. Carbon nuclear magnetic resonance (^{13}C NMR) spectra were recorded using a Bruker AVANCE HD spectrometer at 100 MHz. Chemical shifts are reported in parts per million (ppm) and are calibrated to the solvent peak: carbon ($CDCl_3$, 77.23 ppm). All final compounds were purified by reverse phase HPLC or SFC. The purity for test compounds was determined by HPLC on a LC-20AB Shimadzu instrument. HPLC conditions were as follows: Kinetex C18 LC Column 4.6 × 50 mm, 5 μm, 10−80% MECN (0.0375% TFA) in water (0.01875% TFA), 4 min run, flow rate 1.5 mL/min, UV detection (λ = 220, 215, 254 nm) or XBridge C18, 2.1 × 50 mm, 5 μm, 10−80% MECN in water buffered with 0.025% ammonia, 4 min run, flow rate 0.8 mL/min, UV detection (λ = 220, 215, 254 nm). The mass spectra were obtained using LCMS on a LCMS-2020 Shimadzu instrument using electrospray ionization (ESI). LCMS conditions were as follows: Kinetex EVO C18 30 × 2.1 mm, 5 μm, 5−95% MECN (0.0375% TFA) in water (0.01875% TFA), 1.5 min run, flow rate 1.5 mL/min, UV detection (λ = 220, 254 nm), or Kinetex EVO C18 2.1 × 30 mm, 5 μm, 5−95% MECN in water buffered with 0.025% ammonia, 1.5 min run, flow rate 1.5 mL/min, UV detection (λ = 220, 254 nm). High-resolution mass measurements were carried out on an Agilent 1290LC & 6530Q-TOF series with ESI. Melting point data were recorded on a Mettler Toledo MP70 [start temperature = 65 °C, end temperature = 255 °C, rate (°C/min) = 3.0]. Optical rotation data were recorded on an Anton Paar MCP500 [length = 1 dm, sodium lamp, λ (nm) = 589, temperature = 25 °C]. The SFC purity for test compounds was determined with a Shimadzu LC-30ADsf.

Cell-Based Phospho-ERK Assay. All experiments were performed under standard conditions (37 °C and 5% CO_2). IC_{50} values were calculated by dose response curve fitting using a four-parameter method. NCI-H358 cells harboring the $KRAS^{G12C}$ mutation were seeded in 96-well plates in RPMI supplemented with 10% fetal bovine serum. Plates were incubated overnight. After incubation of cells with an inhibitor for 3 h, cells were washed once with phosphate-buffered saline (PBS), fixed with 3.8% formaldehyde, and permeabilized with ice cold methanol. The plates were then incubated with Li-Cor blocking buffer. Subsequently, phosphorylation of ERK was assessed by an in-cell western method by incubating with primary antibodies against GAPDH (mouse) and phospho-ERK (rabbit). The plates were then incubated with fluorescent secondary antibodies specific for mouse or rabbit. The plates were imaged on a Li-Cor fluorescent plate reader at 680 and 800 nm wavelengths. The phospho-ERK signal was normalized to the GAPDH signal, and POC values were generated.

https://dx.doi.org/10.1021/acs.jmedchem.9b02052
J. Med. Chem. XXXX, XXX, XXX−XXX

Cocrystal Structures. KRAS isoform 4B, residues 1:169, was cloned into *Escherichia coli* with all 3 native cysteines mutated to other residues (C51S, C80L, and C118S) and residue G12 mutated to C. A 6-His tag and a TEV-cleavage site were added to the N-terminus. This is the same $KRAS^{G12C}$ "Lite" construct described in Ostrem et al.[9] *KRAS* protein was expressed in BL21 (DE3) cells and purified by IMAC and ResourceQ chromatography. The 6-His tag was removed by cleavage overnight with TEV protease. In order to ensure complete loading with GDP, the KRAS protein at approximately 500 μM was incubated with 15 mM ethylenediaminetetraacetic acid (EDTA) for 1 h, and 25 mM MgGDP plus 50 mM $MgCl_2$ was then added and incubated for 1 h. The KRAS protein was further purified over a Superdex 75 sizing column. KRAS protein at approximately 260 μM was incubated with a 4-fold molar excess of compound and monitored by mass spectrometry until >95% of the protein was modified by the compound. The protein was then separated from the excess compound on a PD-10 column and concentrated to 16 mg/mL. The protein−ligand complex was crystallized at 20 °C in hanging drops using 2 μL protein + 2 μL precipitant. The precipitant was 32% PEG 4K, 0.1 M NaOAc (unbuffered) and 8% 2-propanol. Crystals were cryoprotected with 15% glycerol and flash frozen. Data were collected in-house on a Rigaku FR-E generator and Pilatus 1M detector.

The structures were solved using the CCP4 suite (https://www.ccp4.ac.uk/) and Coot (https://www2.mrc-lmb.cam.ac.uk/personal/pemsley/coot/). Coordinates have been deposited with PDB accession numbers. Compound **7** Figure 3 6USX. Compound **12a** Figure 4 6USZ. **MRTX849** Figure 12 6UTO.

Computational Modeling. Computational modeling of various inhibitors and illustrations were performed with the Maestro suite of programs available from Schrödinger, LLC, New York, NY, 2019.

In Vivo Studies. All mouse studies were conducted in compliance with all applicable regulations and guidelines of the Institutional Animal Care and Use Committee (IACUC) from the National Institutes of Health (NIH). Mice were maintained under pathogen-free conditions, and food and water were provided ad libitum. 6−8 week-old, female, athymic nude-*Foxn1*^{nu} mice (Envigo, San Diego) were injected subcutaneously with either NCI-H358 or MIA PaCa-2 cells in 100 μL of PBS and Matrigel matrix in the right hind flank with 5.0×10^6 cells (Corning #356237; Discovery Labware, MA) 50:50 cells/Matrigel. Mouse health was monitored daily, and caliper measurements began when tumors were palpable. Tumor volume measurements were determined utilizing the formula $0.5 \times L \times W^2$ in which L refers to length and W refers to the width of each tumor. When tumors reached an average tumor volume of ∼350 mm^3, mice were randomized into treatment groups. Mice were treated by oral gavage with either vehicle consisting of 10% research grade Captisol (CyDex Pharmaceuticals, KS) in 50 mM citrate buffer pH 5.0 or study compound in vehicle at indicated doses. For efficacy studies, animals were orally administered study compound or vehicle and monitored daily, tumors were measured 3 times per week and body weights were measured 2 times per week. Study day on efficacy plots indicates the day after which compound treatment was initiated. For PK/PD studies, tumors and plasma were collected after a single dose at the time points and concentration range indicated.

Inherent GSH Reactivity. Compounds (1 μM) were incubated at 37 °C for one and 4 h in KPB buffer with and without 5 mM GSH. At the end of the designated time point, samples were quenched with acetonitrile spiked with 40 mM NEM and 0.2 μM final concentration of labetalol (internal standard). Samples were centrifuged, and supernatants were analyzed by LC−MS/MS.

$KRAS^{G12C}$ Target Engagement. Tumor fragments were homogenized in 6 M guanidine−HCl, 50 mM *N*-(2-hydroxyethyl)-piperazine-*N*′-ethanesulfonic acid (HEPES) (pH 7.5), and 5 mM TCEP. Following centrifugation, the protein concentration of the supernatant was determined using a Bradford assay. An internal standard ($^{13}C^{15}N$ recombinant $KRAS^{G12C}$) and 20 mM iodoacetamide were added to 200 μg of tumor protein in 200 μL of lysis buffer, and samples were incubated at 37 °C for 30 min in the dark. Following alkylation, 100 μL of the reaction was exchanged into 1 M guanidine−HCl, 50 mM HEPES (pH 7.5), using a 96-well Zeba spin plate. Proteins were digested with 1 μg of trypsin/Lys-C mix at 37 °C for 18 h. Peptides were desalted using a C18 spin plate, and the solvent was removed by evaporation. Peptides were solubilized in 0.1% formic acid, 5% acetonitrile, 95% water, for LCMS analysis. A targeted method on a Sciex TripleTOF instrument was used to monitor the Cys-12-containing $KRAS^{G12C}$ peptide, an internal reference peptide, as well as the corresponding isotope-labeled peptides. $KRAS^{G12C}$ engagement was calculated as previously reported.[13]

Allometric Scaling. Scaling of predicted CL in humans was conducted by an allometric equation relating the body weight of the mouse, rat, monkey, and dog versus CL measured in IV PK experiments. The following functional form of the equation

$$\mathrm{CL} = aW^b$$

where CL is the IV predicted CL, W is the body weight of the organism, a is the coefficient of the allometric equation, and b is the exponent of the allometric equation. The equation is then transformed logarithmically to

$$\log \mathrm{CL} = \log a + b \log W$$

In this form of the equation, log a is equivalent to the y-intercept and b is equivalent to the slope based on a log−log plot of log CL versus log W. The following body weights were assumed for the mouse (0.02 kg), rat (0.3 kg), monkey (5 kg), and dog (10 kg) and were log transformed and plotted against the log of IV CL. A human body weight of 70 kg was assumed, and slope and intercept values described from the linear regression of the log CL versus log WT of the mouse, rat, monkey, and dog were used to predict log CL in the human.

Stability—Liver Cytosol Supplemented with GSH. Compounds (1 μM) were incubated at 37 °C for 30 min in a 1 mg/mL liver cytosol, supplemented with 5 mM GSH in KPB buffer. At the end of the designated time point, samples were quenched with acetonitrile spiked with 40 mM NEM and 0.2 μM concentration of labetalol (internal standard). Samples were centrifuged, and supernatants were analyzed by LC−MS/MS.

Whole Blood Stability. Compounds (5 μM) were incubated at 37 °C for 30, 60, and 240 min in a 1:1 (v/v) blood and PBS, pH 7.4. Diluted blood was preincubated for 15 min at 37 °C and 100% humidity before the reactions were initiated with the dosing of the compound. At the end of each designated time point, the red blood cells were lysed 1:1 with water, mixed at 600 rpm for 1 min, and stopped with acetonitrile containing 0.625 μM labetalol (internal standard). Samples were centrifuged, and supernatants were analyzed by LC−MS/MS.

Measurement of k_{inact}/K_I. Recombinant $KRAS^{G12C}$ "Lite" (C51S/C80L/C118S) was reacted with a range of **MRTX849** concentrations in 25 mM HEPES (pH 7.0), 150 mM NaCl, 5 mM $MgCl_2$, 10 mM octyl β-glucopyranoside, and 0.5 mM TCEP, for 0−45 s, at room temperature. At each time-point, the reaction was quenched with 50 mM HCl, and 0.25 μg of pepsin was added. $KRAS^{G12C}$ was digested for 4 h at 37 °C, and the resulting Cys-12-containing peptide was analyzed by LCMS. The percent of modified $KRAS^{G12C}$ at each time-point was calculated from the 0 s control sample for each concentration of **MRTX849**, and k_{obs} was subsequently calculated from the slope of the ln(POC) versus time data. Rate versus concentration data fit the Michaelis−Menten equation.

Metabolite Identification in Hepatocytes. Cryopreserved hepatocytes from mouse, rat, dog, and human were thawed and diluted to a viable cell density of 1×10^6 cells/mL using Dulbecco's modified Eagle medium. **MRTX849** (10 μM) was added to 1 mL of each hepatocyte suspension, and samples were incubated at 37 °C for 2 h. Metabolism was quenched with the addition of 1% formic acid, samples were centrifuged, and the supernatant was loaded onto a 3cc Oasis HLB cartridge. **MRTX849** and metabolites were washed with 5% methanol in water and eluted with 100% methanol. The solvent was evaporated under a stream of nitrogen gas, and metabolites were reconstituted with 150 μL of 30:70 acetonitrile/water (v/v).

https://dx.doi.org/10.1021/acs.jmedchem.9b02052
J. Med. Chem. XXXX, XXX, XXX−XXX

Metabolites were separated on a Gemini NX-C18 column and detected by absorbance at 290 nm and mass spectrometry. Relative amounts of metabolites were determined by A_{290nm} peak intensity, and the biotransformation was characterized by the associated m/z and MSMS fragmentation patterns.

NCI-H358 Proteome Cysteine Selectivity Assay. NCI-H358 cells were treated with 3 μM **MRTX849** for 3 h and then lysed with 1% NP-40-containing buffer and sonication. Cell extracts were treated with 5 mM iodoacetamide desthiobiotin for 1 h at room temperature. Proteins were precipitated with acetone and resuspended in a buffer containing 6 M guanidine−HCl, 50 mM HEPES, pH 7.5, and 5 mM TCEP and incubated for 15 min at 65 °C. Following treatment with iodoacetamide and buffer exchange into 1 M guanidine-HCl, 50 mM HEPES (pH 7.5), proteins were digested with trypsin/Lys-C overnight. Desthiobiotinylated peptides were enriched using streptavidin agarose and eluted with 50% acetonitrile and 0.1% TFA. The solvent was removed by evaporation and peptides were resuspended in 0.1% formic acid, 5% acetonitrile, and in water. Samples were analyzed on a Sciex 6600 TripleTOF instrument. Protein Pilot 5 was used to identify peptides labeled with desthiobiotin from data-dependent MS/MS scans and relative quantitation (**MTRX849**-treated vs control) was conducted using SWATH analysis.

Click Chemistry Target Identification. Two flasks of NCI-H358 cells (60 million cells/T225 flask) in the RPMI 1640 SILAC light media were treated with DMSO as the control, and two flasks of cells in the RPMI 1640 SILAC heavy media ($^{13}C_6$-lysine, $^{13}C_6$,$^{15}N_4$-arginine) were treated with 1 μM **MRTX849** for 3 h at 37 °C. All cells were then treated with 2 μM compound 24 for 3 h at 37 °C. Cells were then lysed with 50 mM HEPES, 150 NaCl, 0.5% Triton-X 100, 1 mM EDTA, 1 mM EGTA, and HALT protease inhibitor cocktail, for 5 min, probe sonicated, and centrifuged, and the supernatant was filtered with a 45 μm syringe filter. For each replicate, 4 mg of protein in "light"' lysate was combined with 4 mg of protein in "heavy" lysate for sample processing. Proteins were isolated using chloroform/methanol precipitation, resuspended in 0.18% sodium dodecyl sulfate (SDS) in 50 mM HEPES pH 7.5, and 'clicked' to azide agarose by incubating with 5 mM ascorbate, 1 mM $CuSO_4$, and 2 mM BTTAA, for 2.5 h at room temperature. Resin-bound proteins were treated with 10 mM DTT for 40 min and then with 20 mM iodoacetamide for 30 min and washed with (1) 100 mM Tris, pH 8.0, 250 mM NaCl, 1% SDS, 5 mM EDTA, (2) 8 M urea, 100 mM Tris, pH 8.0, and (3) 20% acetonitrile in water. Trypsin/Lys-C (1 μg) was added to the protein-bound resin, suspended in 20 mM Tris pH 8.0, 2 mM $CaCl_2$, 10% acetonitrile, and incubated for 18 h at 37 °C. Eluted peptides were desalted on C18 spin columns, solvent was removed by evaporation, and peptides were resuspended in 0.1% formic acid, 5% acetonitrile, and in water for LCMS analysis. Samples were analyzed on a Sciex 6600 TripleTOF instrument. Protein Pilot 5 was used to identify peptides from data-dependent MS/MS scans of an unlabeled sample, and relative quantitation (MTRX849-treated vs control) was conducted using SWATH analysis of the SILAC samples.

■ ASSOCIATED CONTENT

Supporting Information

The Supporting Information is available free of charge at https://pubs.acs.org/doi/10.1021/acs.jmedchem.9b02052.

Synthetic experimental procedures, NMR spectra of final compounds, GSH reactivity data, metabolism of **MRTX849**, $KRAS^{G12C}$ target engagement, measurement of K_{inact}/K_I, metabolite identification in hepatocytes, NCI-H358 proteome cysteine selectivity assay, and click chemistry target identification and proteome selectivity and click chemistry target identification quantified protein list (PDF)

Molecular formula strings (CSV)

■ AUTHOR INFORMATION

Corresponding Authors

Jay B. Fell − *Array BioPharma Inc, Boulder, Colorado 80301, United States;* orcid.org/0000-0002-5770-1225; Phone: 303-386-1528; Email: brad.fell@arraybiopharma.com

Matthew A. Marx − *Mirati Therapeutics, San Diego, California 92121, United States;* orcid.org/0000-0003-2351-4787; Phone: 858-332-3558; Email: marxm@mirati.com

Authors

John P. Fischer − *Array BioPharma Inc, Boulder, Colorado 80301, United States*

Brian R. Baer − *Array BioPharma Inc, Boulder, Colorado 80301, United States*

James F. Blake − *Array BioPharma Inc, Boulder, Colorado 80301, United States*

Karyn Bouhana − *Array BioPharma Inc, Boulder, Colorado 80301, United States*

David M. Briere − *Mirati Therapeutics, San Diego, California 92121, United States*

Karin D. Brown − *Array BioPharma Inc, Boulder, Colorado 80301, United States*

Laurence E. Burgess − *Array BioPharma Inc, Boulder, Colorado 80301, United States*

Aaron C. Burns − *Mirati Therapeutics, San Diego, California 92121, United States*

Michael R. Burkard − *Array BioPharma Inc, Boulder, Colorado 80301, United States*

Harrah Chiang − *Mirati Therapeutics, San Diego, California 92121, United States*

Mark J. Chicarelli − *Array BioPharma Inc, Boulder, Colorado 80301, United States*

Adam W. Cook − *Array BioPharma Inc, Boulder, Colorado 80301, United States*

John J. Gaudino − *Array BioPharma Inc, Boulder, Colorado 80301, United States*

Jill Hallin − *Mirati Therapeutics, San Diego, California 92121, United States*

Lauren Hanson − *Array BioPharma Inc, Boulder, Colorado 80301, United States*

Dylan P. Hartley − *Array BioPharma Inc, Boulder, Colorado 80301, United States*

Erik J. Hicken − *Array BioPharma Inc, Boulder, Colorado 80301, United States*

Gary P. Hingorani − *Array BioPharma Inc, Boulder, Colorado 80301, United States*

Ronald J. Hinklin − *Array BioPharma Inc, Boulder, Colorado 80301, United States*

Macedonio J. Mejia − *Array BioPharma Inc, Boulder, Colorado 80301, United States*

Peter Olson − *Mirati Therapeutics, San Diego, California 92121, United States*

Jennifer N. Otten − *Array BioPharma Inc, Boulder, Colorado 80301, United States*

Susan P. Rhodes − *Array BioPharma Inc, Boulder, Colorado 80301, United States*

Martha E. Rodriguez − *Array BioPharma Inc, Boulder, Colorado 80301, United States*

Pavel Savechenkov − *Array BioPharma Inc, Boulder, Colorado 80301, United States*

Darin J. Smith − *Array BioPharma Inc, Boulder, Colorado 80301, United States*

https://dx.doi.org/10.1021/acs.jmedchem.9b02052
J. Med. Chem. XXXX, XXX, XXX−XXX

Niranjan Sudhakar − *Mirati Therapeutics, San Diego, California 92121, United States*
Francis X. Sullivan − *Array BioPharma Inc, Boulder, Colorado 80301, United States*
Tony P. Tang − *Array BioPharma Inc, Boulder, Colorado 80301, United States*
Guy P. Vigers − *Array BioPharma Inc, Boulder, Colorado 80301, United States*
Lance Wollenberg − *Array BioPharma Inc, Boulder, Colorado 80301, United States*
James G. Christensen − *Mirati Therapeutics, San Diego, California 92121, United States*

Complete contact information is available at: https://pubs.acs.org/10.1021/acs.jmedchem.9b02052

Author Contributions

The manuscript was written through contributions of all authors. All authors have given approval to the final version of the manuscript.

Notes

The authors declare no competing financial interest.

■ ACKNOWLEDGMENTS

We would like to thank the IDSU chemistry team from WuXi AppTec in Wuhan, China for their valuable contributions to this work. We are particularly grateful to Tao Guo, Duan Liu, Jie Qu, Yanchun Shen, Kunz Yang, Feng Zhao, and Yaolong Zhang.

■ ABBREVIATIONS

ADME, absorption, distribution, metabolism, and excretion; AUC_{inf}, area under the curve extrapolated to infinity; CL, clearance; C_{max}, maximum concentration; *F*, bioavailability; FaSSIF, fasted state simulated intestinal fluid; GSH, glutathione; LCMS, liquid chromatography mass spectrometry; P-gp, P-glycoprotein; PK, pharmacokinetics; PPB, plasma protein binding; SWATH, sequential windowed acquisition of all theoretical fragment ions; SILAC, stable isotope labeling with amino acids in cell culture; TCEP, tris(2-carboxyethyl)-phosphine hydrochloride; T_{max}, time at C_{max}; TGI, tumor growth inhibition

■ REFERENCES

(1) Bos, J. Ras oncogenes in human cancer: a review. *Cancer Res.* **1989**, *49*, 4682−4689.
(2) Jarvis, L. Have drug hunters finally cracked KRAS? *Chem. Eng. News* **2016**, *94*, 28−33.
(3) John, J.; Sohmen, R.; Feuerstein, J.; Linke, R.; Wittinghofer, A.; Goody, R. S. Kinetics of interaction of nucleotides with nucleotide-free H-ras p21. *Biochemistry* **1990**, *29*, 6058−6065.
(4) Matikas, A.; Mistriotis, D.; Georgoulias, V.; Kotsakis, A. Targeting KRAS mutated non-small cell lung cancer: A history of failures and a future of hope for a diverse entity. *Crit. Rev. Oncol. Hematol.* **2017**, *110*, 1−12.
(5) Sanchez-Vega, F.; Mina, M.; Armenia, J.; Chatila, W. K.; Luna, A.; La, K. C.; Dimitriadow, S.; Liu, D. L.; Kantheti, H. S.; Saghafinia, S.; Chakravarty, D.; Daian, F.; Gao, Q.; Bailey, M. H.; Liang, W. W.; Foltz, S. M.; Shmulevich, I.; Ding, L.; Heins, Z.; Ochoa, A.; Gross, B.; Gao, J.; Zhang, H.; Kundra, R.; Kandoth, C.; Bahceci, I.; Dervishi, L.; Dogrusoz, U.; Zhou, W.; Shen, H.; Laird, P. W.; Way, G. P.; Greene, C. S.; Liang, H.; Xiao, Y.; Wang, C.; Iavarone, A.; Berger, A. H.; Bivona, T. G.; Lazar, A. J.; Hammer, G. D.; Giordano, T.; Kwong, L. N.; McArthur, G.; Huang, C.; Tward, A. D.; Frederick, M. J.; McCormick, F.; Meyerson, M.; Van Allen, E. M.; Cherniack, A. D.; Ciriello, G.; Sander, C.; Schultz, N. Oncogenic signaling pathways in the cancer genome atlas. *Cell* **2018**, *172*, 321−337.
(6) Simanshu, D. K.; Nissley, D. V.; McCormick, F. Ras proteins and their regulators in human disease. *Cell* **2017**, *170*, 17−33.
(7) Ledford, H. Cancer: The Ras renaissance. *Nature* **2015**, *520*, 278−280.
(8) Papke, B.; Der, C. J. Drugging RAS: Know the enemy. *Science* **2017**, *355*, 1158−1163.
(9) Ostrem, J. M.; Peters, U.; Sos, M. L.; Wells, J. A.; Shokat, K. M. K-Ras (G12C) inhibitors allosterically control GTP affinity and effector interactions. *Nature* **2013**, *503*, 548−551.
(10) Ostrem, J. M. L.; Shokat, K. M. Direct small-molecule inhibitors of KRAS: from structural insights to mechanism-based design. *Nat. Rev. Drug Discov.* **2016**, *15*, 771−785.
(11) Janes, M. R.; Zhang, J.; Li, L.-S.; Hansen, R.; Peters, U.; Guo, X.; Chen, Y.; Babbar, A.; Firdaus, S. J.; Darjania, L.; Feng, J.; Chen, J. H.; Li, S.; Li, S.; Long, Y. O.; Thach, C.; Liu, Y.; Zarieh, A.; Ely, T.; Kucharski, J. M.; Kessler, L. V.; Wu, T.; Yu, K.; Wang, Y.; Yao, Y.; Deng, X.; Zarrinkar, P. P.; Brehmer, D.; Dhanak, D.; Lorenzi, M. V.; Hu-Lowe, D.; Patricelli, M. P.; Ren, P.; Liu, Y. Targeting KRAS mutant cancers with a covalent G12C-specific inhibitor. *Cell* **2018**, *172*, 578−589.e17.
(12) Patricelli, M. P.; Janes, M. R.; Li, L.-S.; Hansen, R.; Peters, U.; Kessler, L. V.; Chen, Y.; Kucharski, J. M.; Feng, J.; Ely, T.; Chen, J. H.; Firdaus, S. J.; Babbar, A.; Ren, P.; Liu, Y. Selective inhibition of oncogenic KRAS output with small molecules targeting the inactive state. *Canc. Discov.* **2016**, *6*, 316−329.
(13) Lito, P.; Solomon, M.; Li, L.-S.; Hansen, R.; Rosen, N. Allele-specific inhibitors inactivate mutant KRAS G12C by a trapping mechanism. *Science* **2016**, *351*, 604−608.
(14) Fell, J. B.; Fischer, J. P.; Baer, B. R.; Ballard, J.; Blake, J. F.; Bouhana, K.; Brandhuber, B. J.; Briere, D. M.; Burgess, L. E.; Burkard, M. R.; Chiang, H.; Chicarelli, M. J.; Davidson, K.; Gaudino, J. J.; Hallin, J.; Hanson, L.; Hee, K.; Hicken, E. J.; Hinklin, R. J.; Marx, M. A.; Mejia, M. J.; Olson, P.; Savechenkov, P.; Sudhakar, N.; Tang, T. P.; Vigers, G. P.; Zecca, H.; Christensen, J. G. Discovery of tetrahydropyridopyrimidines as irreversible covalent inhibitors of KRAS-G12C with in vivo activity. *ACS Med. Chem. Lett.* **2018**, *9*, 1230−1234.
(15) Berenbom, M.; Young, L. Biochemical Studies of Toxic Agents. 3. The Isolation of 1- and 2-Naphthyl-sulphuric acid and 1- and 2-naphthylglucaronide from the urine of rats dosed with 1- and 2-naphthol. *Biochem. J.* **1951**, *49*, 165−169.
(16) Michel, J.; Tirado-Rives, J.; Jorgensen, W. L. Energetics of displacing water molecules from protein binding sites: consequences for ligand optimization. *J. Am. Chem. Soc.* **2009**, *131*, 15403−15411.
(17) Marx, M.; Baer, B. R.; Ballard, J.; Blake, J. F.; Bouhana, K.; Briere, D. M.; Burgess, L. E.; Burkard, M. R.; Chiang, H.; Chicarelli, M. J.; Christensen, J. G.; Cook, A. W.; Fischer, J. P.; Hallin, J.; Mejia, M. J.; Olson, P.; Rodriguez, M.; Savenchenkov, P.; Sudhakar, N.; Tang, T. P.; Vigers, G. P.; Fell, J. B. Structure based drug discovery of MRTX1257, a selective, covalent KRAS G12C inhibitor with oral activity in animal models of cancer. *AACR Targeting RAS-Driven Cancers*, 2018, San Diego CA. Hallin, J.; Aranda, R.; Baer, B. R.; Burkard, M. R.; Calinisan, A.; Chiang, H.; Engstrom, L. D.; Fell, J. B.; Marx, M. A.; Olson, P.; Christensen, J. G. Insight towards therapeutic susceptibility of KRAS mutant cancers from MRTX1257; A prototype selective inhibitor of KRAS G12C. *AACR Targeting RAS-Driven Cancers*, 2018, San Diego CA.
(18) Mahmood, I. Application of allometric principles for the prediction of pharmacokinetics in human and veterinary drug development. *Adv. Drug Deliv. Rev.* **2007**, *59*, 1177−1192.
(19) Davies, B.; Morris, T. Physiological parameters in laboratory animals and humans. *Pharm. Res.* **1993**, *10*, 1093−1095.
(20) Shibata, Y.; Chiba, M. The role of extrahepatic metabolism in the pharmacokinetics of the targeted covalent inhibitors afatinib, ibrutinib, and neratinib. *Drug Metab. Dispos.* **2015**, *43*, 375−384.
(21) Leung, L.; Yang, X.; Strelevitz, T. J.; Montgomery, J.; Brown, M. F.; Zientek, M. A.; Banfield, C.; Gilbert, A. M.; Thorarensen, A.;

Dowty, M. E. Clearance prediction of targeted covalent inhibitors by in vitro-in vivo extrapolation of hepatic and extrapatic clearance mechanisms. *Drug Metab. Dispos.* **2017**, *45*, 1−7.
(22) Xia, G.; Chen, W.; Zhang, J.; Shao, J.; Zhang, Y.; Huang, W.; Zhang, L.; Qi, W.; Sun, X.; Li, B.; Xiang, Z.; Ma, C.; Xu, J.; Deng, H.; Li, Y.; Li, P.; Miao, H.; Han, J.; Liu, Y.; Shen, J.; Yu, Y. A chemical tuned strategy to develop novel irreversible EGFR-TK inhibitors with improved safety and pharmacokinetic profiles. *J. Med. Chem.* **2014**, *57*, 9889−9900.
(23) Zhao, B.; Xiao, Z.; Qi, J.; Luo, R.; Lan, Z.; Zhang, Y.; Hu, X.; Tang, Q.; Zheng, P.; Xu, S.; Zhu, W. Design, synthesis and biological evaluation of AZD9291 derivatives as selective and potent $EGFRL^{858R/T790M}$ inhibitors. *Eur. J. Med. Chem.* **2019**, *163*, 367−380.
(24) Hansen, R.; Peters, U.; Babbar, A.; Chen, Y.; Feng, J.; Janes, M. R.; Li, L.-S.; Ren, P.; Liu, Y.; Zarrinkar, P. P. The reactivity driven biochemical mechanism of covalent KRAS(G12C) inhibitors. *Nat. Struct. Mol. Biol.* **2018**, *25*, 454−462.
(25) Canon, J.; Rex, K.; Saiki, A. Y.; Mohr, C.; Cooke, K.; Bagal, D.; Gaida, K.; Holt, T.; Knutson, C. G.; Koppada, N.; Lanman, B. A.; Werner, J.; Rapaport, A. S.; San Miguel, T.; Ortiz, R.; Osgood, T.; Sun, J.-R.; Zhu, X.; McCarter, J. D.; Volak, L. P.; Houk, B. E.; Fakih, M. G.; O'Neil, B. H.; Price, T. J.; Falchook, G. S.; Desai, J.; Kuo, J.; Govindan, R.; Hong, D. S.; Ouyang, W.; Henary, H.; Arvedson, T.; Cee, V. J.; Lipford, J. R. The clinical KRAS(G12C) inhibitor AMG 510 drives anti-tumour immunity. *Nature* **2019**, *575*, 217−223.
(26) Wijeratne, A.; Xiao, J.; Reutter, C.; Furness, K. W.; Leon, R.; Zia-Ebrahimi, M.; Cavitt, R. N.; Strelow, J. M.; Van Horn, R. D.; Peng, S.-B.; Barda, D. A.; Engler, T. A.; Chalmers, M. J. Chemical proteomic characterization of a covalent KRASG12C inhibitor. *ACS Med. Chem. Lett.* **2018**, *9*, 557−562.
(27) Hallin, J.; Engstrom, L. D.; Hargis, L.; Calinisan, A.; Aranda, R.; Briere, D. M.; Sudhakar, N.; Bowcut, V.; Baer, B. R.; Ballard, J. A.; Burkard, M. R.; Fell, J. B.; Fischer, J. P.; Vigers, G. P.; Xue, Y.; Gatto, S.; Fernandez-Banet, J.; Pavlicek, A.; Velastagui, K.; Chao, R. C.; Barton, J.; Pierobon, M.; Baldelli, E.; Patricoin, E. F.; Cassidy, D. P.; Marx, M. A.; Rybkin, I. I.; Johnson, M. L.; Ou, S.-H. I.; Lito, P.; Papadopoulos, K. P.; Jänne, P. A.; Olson, P.; Christensen, J. G. The KRASG12C inhibitor, MRTX849, provides insights toward therapeutic susceptibility of KRAS mutant cancers in mouse models and patients. *Canc. Discov.* **2020**, *10*, 54−71.
(28) Cheung, C. W.; Buchwald, S. L. Mild and General Palladium-Catalyzed Synthesis of Methyl Ethers Enabled by Palladacycle Precatalyst. *Org. Lett.* **2013**, *15*, 3998. Wu, X.; Fors, B. P.; Buchwald, S. L. A single phosphine ligand allows palladium-catalyzed intermolecular C-O bond formation with secondary and primary alcohols. *Angew. Chem., Int. Ed.* **2011**, *50*, 9943. Maligres, P. E.; Li, J.; Krska, S. W.; Schreier, J. D.; Raheem, I. T. C-O cross-coupling of activated aryl and heteroaryl halides with aliphatic alcohols. *Angew. Chem., Int. Ed.* **2012**, *51*, 9071.
(29) Sureshbabu, V. V.; Vishwanatha, T. M.; Panguluri, N. R.; Basavaprabhu. Propanephosphonic acid anhydride (T3P®) - a benign reagent for diverse applications inclusive of large-scale synthesis. *Synthesis* **2013**, *45*, 1569−1601.

https://dx.doi.org/10.1021/acs.jmedchem.9b02052
J. Med. Chem. XXXX, XXX, XXX−XXX